

2.5. ELECTRON DIFFRACTION AND ELECTRON MICROSCOPY IN STRUCTURE DETERMINATION

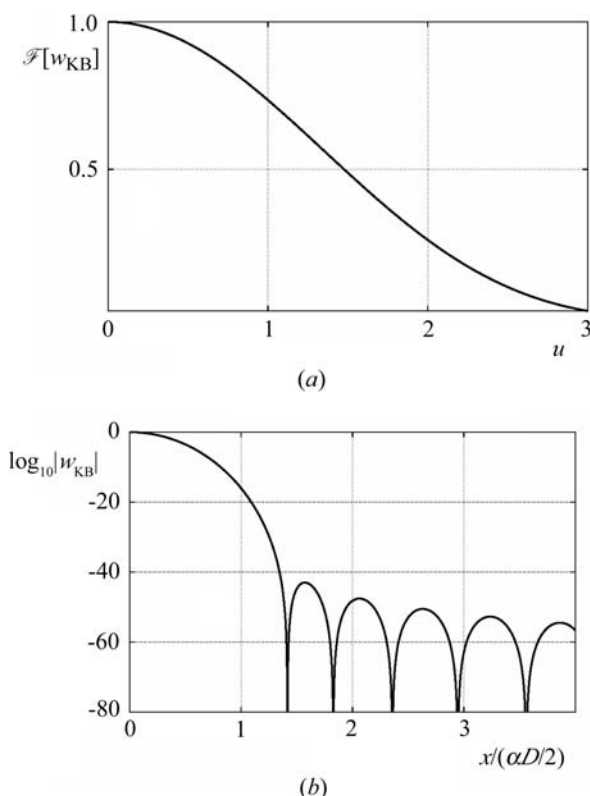


Fig. 2.5.6.6. Kaiser–Bessel window function used in the gridding reconstruction algorithm GDFR. (a) In Fourier space, the window function is effectively zero outside the support of six Fourier pixels. (b) In real space, the zeros of the window function are beyond the radius of the reconstructed object.

vecchia *et al.*, 1993). Unfortunately, the recommended window size makes them impractical for most applications.

The most accurate Fourier reconstruction methods are those that employ nonuniform Fourier transforms, particularly the 3D gridding method (O’Sullivan, 1985; Schomberg & Timmer, 1995). The gridding-based direct Fourier reconstruction algorithm (GDFR) (Penczek *et al.*, 2004) was developed specifically for single-particle reconstruction. It comprises three steps:

(1) The first step, known as ‘gridding’, involves calculating for the Fourier transform of each projection the convolution

$$\sum_i \mathcal{F}[w] * (c\mathcal{F}[\varphi_2]), \quad (2.5.6.41)$$

where c are ‘gridding weights’ designed to compensate for the nonuniform distribution of the grid points and $\mathcal{F}[w]$ is an appropriately chosen convolution kernel. After processing all projections, this step yields samples of $\mathcal{F}[w] * \mathcal{F}[\varphi_3]$ on a Cartesian grid.

(2) 3D inverse FFT is used to compute

$$w\varphi_3 = \mathcal{F}^{-1}[\mathcal{F}[w] * \mathcal{F}[\varphi_3]] \quad (2.5.6.42)$$

on a Cartesian grid.

(3) The weights are removed using division:

$$\varphi_3 = w\varphi_3/w. \quad (2.5.6.43)$$

The method involves a number of parameters. First, we need to decide the oversampling factor for the padding with zeros of input projections before FFTs are computed. In GDFR, the

oversampling is set to two, although smaller factors can also yield good results. Second, we need a *window function* $\mathcal{F}[w]$ whose support in Fourier space is ‘small’. In order to assure good computational efficiency of the convolution step (2.5.6.41), in GDFR this support was set to six Fourier voxels. In addition, in order to prevent division by zeros in (2.5.6.43), the *weighting function* $w = \mathcal{F}^{-1}[\mathcal{F}[w]]$ must be positive within the support of the reconstructed object. A recommendable window function is the separable, bell-shaped Kaiser–Bessel window (O’Sullivan, 1985; Jackson *et al.*, 1991; Schomberg & Timmer, 1995) (Fig. 2.5.6.6a):

$$\mathcal{F}[w_{\text{KB}}(\mathbf{u})] = \begin{cases} \prod_{v=1}^d \frac{I_0\{\pi D\alpha s_v [1 - (u_v/s_v)^2]^{1/2}\}}{2s_v}, & \mathbf{u} \in [-\mathbf{s}, \mathbf{s}], \\ 0, & \mathbf{u} \notin [-\mathbf{s}, \mathbf{s}], \end{cases} \quad (2.5.6.44)$$

where I_0 is the zero-order modified Bessel function and $\alpha = 1.25$ is a parameter. The weighting function associated with $\mathcal{F}[w_{\text{KB}}]$ is

$$w_{\text{KB}}(\mathbf{x}) = \prod_{v=1}^d \frac{\sinh[\pi D\alpha s_v (1 - \{x_v/[\alpha(D/2)]^2\})^{1/2}]}{\pi D\alpha s_v (1 - \{x_v/[\alpha(D/2)]^2\})^{1/2}}. \quad (2.5.6.45)$$

Finally, the gridding weights c are chosen such that in discrete implementation of (2.5.6.41) and (2.5.6.42) we obtain a Riemann sum approximating the respective integral (Schomberg, 2002). The Voronoi diagram (Okabe *et al.*, 2000) of the sampling points provides a good partitioning of sampling space, so the gridding weights c are computed by constructing a Voronoi diagram of the grid points and by choosing the weights as the volumes of the Voronoi cells (Fig. 2.5.6.7a). In cryo-EM, the number of projections, thus the number of sampling points in Fourier space, is extremely large. Thus, although the calculation of the gridding weights *via* the 3D Voronoi diagram of the nonuniformly spaced grid points for $\mathcal{F}[\varphi_3]$ would lead to an accurate direct Fourier method, the method would be very slow and would require excessive computer memory. To circumvent this problem, in GDFR (Penczek *et al.*, 2004) the 2D reverse gridding method is used to compute the Fourier transform of each projection on a 2D polar grid. In this way, $\mathcal{F}[\varphi_3]$ is obtained on a 3D spherical grid, where the grid points are located both on centred spheres and on straight lines through the origin. Accordingly, it becomes possible to partition the sampled region into suitable sampling cells *via* the computation of a 2D Voronoi diagram on a unit sphere, rather than a 3D Voronoi diagram in Euclidean space (Fig. 2.5.6.7b). This significantly reduces the memory requirements and improves the computational efficiency of the method, particularly when a fast $O(n \log n)$ algorithm for computing the Voronoi diagram on the unit sphere is employed (Renka, 1997).

The gridding weights in GDFR correspond to the weighting functions in filtered backprojection algorithms. Moreover, setting the gridding weights to be equal to angular regions on the unit sphere directly corresponds to the equating of weighting function (2.5.6.29) in 2D filtered backprojection to the length of an arc on a unitary circle. Thus, both methods yield nearly optimum projection density functions.

The reversed gridding method is obtained by reversing the sequence of steps (1)–(3) of the gridding method:

(1) the input image is divided by the weighting function φ_2/w ;

(2) the image is padded with zeros and 2D FFT is used to compute $\mathcal{F}[\varphi_2/w]$;

(3) gridding is used to compute $\mathcal{F}[w] * \mathcal{F}[\varphi_2/w]$ on an arbitrary nonuniform grid.